Article

Effects of Hydrothermal Aging on CO and NO Oxidation Activity Over Monometallic and Bimetallic Pt-Pd Catalysts

Jochen Schütz [1,†], Heike Störmer [2], Patrick Lott [1] and Olaf Deutschmann [1,*]

[1] Institute for Chemical Technology and Polymer Chemistry (ITCP), Karlsruhe Institute of Technology (KIT), 76131 Karlsruhe, Germany; schuetz@dvgw-ebi.de (J.S.); patrick.lott@kit.edu (P.L.)

[2] Laboratory for Electron Microscopy (LEM), Karlsruhe Institute of Technology (KIT), 76131 Karlsruhe, Germany; heike.stoermer@kit.edu;

[*] Correspondence: deutschmann@kit.edu; Tel.: +49-72-160-843-064

[†] Current Affiliation: Engler-Bunte-Institut (EBI), Karlsruhe Institute of Technology (KIT), 76131 Karlsruhe, Germany

Abstract: By combining scanning transmission electron microscopy, CO chemisorption, and energy dispersive X-ray spectroscopy with CO and NO oxidation light-off measurements we investigated deactivation phenomena of Pt/Al_2O_3, Pd/Al_2O_3, and $Pt-Pd/Al_2O_3$ model diesel oxidation catalysts during stepwise hydrothermal aging. Aging induces significant particle sintering that results in a decline of the catalytic activity for all catalyst formulations. While the initial aging step caused the most pronounced deactivation and sintering due to Ostwald ripening, the deactivation rates decline during further aging and the catalyst stabilizes at a low level of activity. Most importantly, we observed pronounced morphological changes for the bimetallic catalyst sample: hydrothermal aging at 750 °C causes a stepwise transformation of the Pt-Pd alloy via core-shell structures into inhomogeneous agglomerates of palladium and platinum. Our study shines a light on the aging behavior of noble metal catalysts under industrially relevant conditions and particularly underscores the highly complex transformation of bimetallic Pt-Pd diesel oxidation catalysts during hydrothermal treatment.

Keywords: aging; bimetallic catalyst; catalyst deactivation; diesel oxidation catalyst; palladium; platinum

1. Introduction

Tightening environmental legislation and more stringent emission standards continuously increase the demand for highly active and durable exhaust gas after-treatment systems. Although decades of intense research efforts resulted in the development of catalytic converters with a high initial activity, catalyst deactivation due to poisoning and hydrothermal aging still poses a challenge. Understanding the degradation mechanisms that result in catalyst deactivation is a crucial step towards an increase of catalyst durability, which ultimately allows for saving expensive noble metals. In this context, two of the most commonly used materials in exhaust gas catalysis are platinum and palladium [1], which are particularly exploited for diesel oxidation catalysts (DOCs) [2]. Numerous scientific studies contributed to continuous improvements of DOCs for oxidizing NO, hydrocarbons (HCs) and CO, and today DOCs are an integral part of almost every emission control system for lean-operated internal combustion engines [3,4].

Historically, oxidation catalysts predominantly consisted of platinum, consequently a great variety of studies deal with platinum-based DOCs. In this regard, particle size, particle morphology, oxidation state, and noble metal support interactions are major factors governing CO, HC, and NO conversion [5–11]. For Pt/Al_2O_3, for instance, systematic investigations on the influence of particle size and shape on the catalytic activity revealed

an optimal Pt particle size of approximately 3–4 nm for NO oxidation [6,12], whereas slightly smaller particles with a diameter of 2–3 nm were reported to be most active for CO oxidation [12,13]. Moreover, reduced Pt sites have been identified as the active species for oxidation reactions [14–17]. In addition to the oxidation state, the support material can also tremendously influence both the reaction pathway and catalytic activity [14,18–21]. Gänzler et al. [22] utilized such fundamental insights for rational in situ tuning of the active sites of a Pt/CeO$_2$ DOC in order to enhance its catalytic activity for CO oxidation. As recently summarized in a review article by Datye and Votsmeier [23], also the catalyst preparation and the optimization of the catalyst formulation can maximize activity and stability.

In this context, continuous catalyst improvement by combining different catalytically active materials are an essential aspect of environmental research and can substantially improve heterogeneous catalysts [24]. Although palladium shows only minor NO oxidation activity, its combination with platinum can serve as an effective measure to minimize deactivation phenomena for diesel oxidation catalysts [25–29]. Moreover, palladium shows higher thermal stability under oxidizing conditions compared to oxidized platinum, as the latter one forms volatile PtO$_2$; hence, the usage of a Pt-Pd alloy has been reported as an efficient approach to increase the catalyst's thermal stability [30–33]. Especially the formation of anomalously large Pt particles, which typically occurs during high-temperature treatment of platinum catalysts due to a vapor-phase transport of platinum, can be suppressed by the addition of palladium [30,34]. In contrast, palladium was reported to sinter more rapidly in reducing or inert atmosphere [35], which can be traced back to the formation of metallic palladium that exhibits a lower surface tension than its oxide form [36,37]. Carrillo et al. [38] reported that PdO nanoparticles can trap mobile Pt species under oxidizing conditions, which is of high relevance for understanding the behavior of bimetallic Pt-Pd catalysts. Lately, a wide variety of advanced materials has been proposed for catalytic emission control under lean conditions, namely encapsulated core-shell catalysts [25,39,40] and nanostructured architectures [41,42] for oxidation reactions and microporous materials for NO$_x$ control [43–46]. Although these materials often show extremely promising catalytic activity or stability, fundamental in-depth understanding, transfer into industrial application and upscaling of preparation procedures remains challenging. Gaining profound insights into aging phenomena and ultimately preventing the sintering of catalytically active species represents one of these challenges [47–49]. In the pursuit of providing the community with a profound and comprehensive summary on particle sintering, Hansen et al. [50] derived some general trends for metal nanoparticles of heterogeneous catalysts and identified three different phases of particle growth: Ostwald ripening induces the most substantial deactivation during the first phase and particularly results in disappearance of very small particles. Particle migration and coalescence and Ostwald ripening occur in parallel during the second phase and cause less rapid aging before the catalyst's state and activity stabilizes with only slow sintering during phase three. In this last phase, phenomena such as support restructuring dominate the aging behavior rather than changes of the noble metal component. From a fundamental point of view, kinetics of crystallite sintering suggest that particle migration dominates if the interactions within a noble metal particle are stronger than the noble metal-support interactions [51], which can be exploited for designing durable catalyst systems.

In our present study, we investigated the influence of hydrothermal aging on monometallic Pt and Pd diesel oxidation catalysts and compared the results with alloyed Pt-Pd nanoparticles concerning their morphology and deactivation behavior. While lab-bench catalyst tests served as the premier method for evaluating the conversion efficiency, the noble metal particles were thoroughly characterized by scanning transmission electron microscopy (STEM). Besides evaluation of the noble metal particle size distribution, the alloying level of bimetallic samples was systematically investigated by means of energy dispersive X-ray spectroscopy (EDXS). Herewith we aim to contribute to a holistic under-

standing of degradation pathways of bimetallic platinum-palladium-based diesel oxidation catalysts, which is an integral step towards further improvement of state-of-the-art exhaust gas after-treatment systems.

2. Results

During our experimental study we systematically aged three different model diesel oxidation catalysts (DOC), namely Pt/Al_2O_3, Pd/Al_2O_3, and $Pt-Pd/Al_2O_3$, by exposure to a gas mixture of 400 ppm CO, 100 ppm C_3H_6, 7% CO_2, 12% O_2, 10% H_2O, and balance N_2 at 750 °C, using a gas hourly space velocity (GHSV) of 20 000 h^{-1}. Stepwise aging and subsequent characterization and kinetic testing provide snapshots on the catalyst state during the course of the aging experiment. As presented below, we followed the aging-induced catalyst changes by determining trends of the particle size distribution and dispersion, by investigating the particle morphology and, last but not least, by evaluating the catalytic activity during kinetic tests in model gas mixtures. Details on methodology and conditions can be found in Section 5.

2.1. Particle Size Distribution and Dispersion

To investigate the trend of noble metal dispersion during the course of the stepwise aging procedure, every sample was analyzed in the fresh state and after aging for 1 h, 5 h and 16 h. With a noble metal dispersion of approximately 20%, $Pt-Pd/Al_2O_3$ showed the highest initial dispersion, while the monometallic Pd/Al_2O_3 and Pt/Al_2O_3 exhibited a dispersion of approximately 9%. After exposure to the reaction gas mixture for 1 h, especially $Pt-Pd/Al_2O_3$ showed a pronounced decrease of the dispersion to 12%, whereas during the same time the dispersion of Pt/Al_2O_3 and Pd/Al_2O_3 decreased to 7% and 8%, respectively. According to the chemisorption measurements, further aging causes further moderate sintering of the particles, ultimately resulting in a dispersion of 7% for $Pt-Pd/Al_2O_3$ and 5% for each of the monometallic samples. Comparing the overall trend of the dispersion versus time on stream as shown in Figure 1 reveals that the first hour of aging has the most significant impact on the catalyst. After 5 h of aging, the decrease in dispersion is less pronounced, suggesting a stabilization of the catalysts' dispersion after strong initial changes.
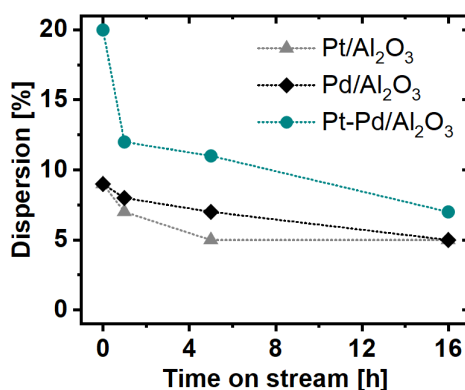

Figure 1. Noble metal dispersion obtained by CO chemisorption measurements during the course of hydrothermal aging.

CO chemisorption is a characterization technique that yields an average value for the noble metal dispersion, but does not allow gaining information on the distribution of particle sizes. Hence, we analyzed a series of representative scanning transmission electron microscopy (STEM) images, which provides more detailed insights into the evolution of

the particle size distribution for the different catalysts during the course of the aging series. Figure 2 summarizes these findings and Table 1 compares the results obtained by CO chemisorption and electron microscopy. In this context, Equation (1) allows calculating the mean particle diameter d_D from the dispersion values obtained by CO chemisorption,

$$d_D = \frac{1.11}{D},$$ (1)

with the mean particle diameter d_D given in nm and D as the dimensionless noble metal dispersion ($0 < D < 1$). Equation (1) assumes a hemispherical shape of the supported noble metal particles and is based on characteristic structural parameters of palladium and platinum [52].
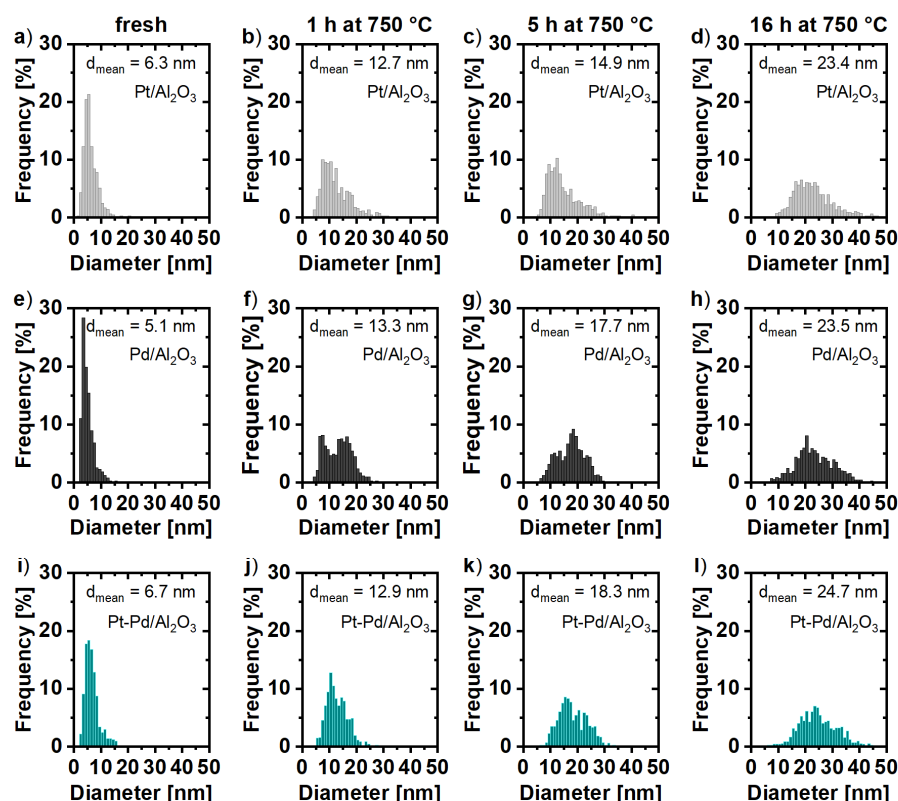

Figure 2. Particle size distribution for Pt/Al₂O₃ (**a–d**), Pd/Al₂O₃ (**e–h**), and Pt-Pd/Al₂O₃ (**i–l**) in the fresh state and after hydrothermal aging for 1 h, 5 h, and 16 h.

Table 1. Mean noble metal particle size during the course of the aging experiment obtained by scanning transmission electron microscopy (STEM) analysis of approximately 650 particles and calculated according to Equation (1) based on the dispersion values obtained by means of CO chemisorption.

	Mean particle size [nm]			
Catalyst	fresh	1 h, 750 °C	5 h, 750 °C	16 h, 750 °C
Pt/Al₂O₃	6.3 ± 2.9 [1]	12.7 ± 5.7 [1]	14.9 ± 6.2 [1]	23.4 ± 8.1 [1]
	12.3 [2]	15.9 [2]	22.2 [2]	22.2 [2]
Pd/Al₂O₃	5.1 ± 2.2 [1]	13.3 ± 4.9 [1]	17.7 ± 5.5 [1]	23.5 ± 7.0 [1]
	12.3 [2]	13.9 [2]	15.9 [2]	22.2 [2]
Pt-Pd/Al₂O₃	6.7 ± 2.6 [1]	12.9 ± 3.9 [1]	18.3 ± 5.2 [1]	24.7 ± 6.9 [1]
	5.55 [2]	9.25 [2]	10.1 [2]	15.9 [2]

[1] based on TEM results; [2] based on CO chemisorption results.

In line with the dispersion values obtained by CO chemisorption, STEM also revealed a significant particle sintering due to the aging at 750 °C, irrespective of the catalyst formulation. While for the monometallic Pt catalyst an initial particle size of 6.3 nm was found in the fresh state, 16 h of hydrothermal aging resulted in a mean particle size of 23.4 nm. Similarly, Pd/Al$_2$O$_3$ exhibited a mean particle size of 5.1 nm in the fresh state and 23.5 nm after 16 h of hydrothermal aging, respectively. Although previous findings point to a higher sintering resistance of bimetallic Pd-Pt oxidation catalysts, [28] the mean particle size diameter for the bimetallic noble metal particles increased from 6.7 nm to 24.8 nm in our aging experiments. The STEM images confirm the findings from the CO chemisorption measurements that the most pronounced particle size increase occurs during the first hour of aging, followed by a gradual further increase during the following hours. Besides simple sintering, the aging also induces changes of the particle size distribution, which is initially rather narrow in the fresh state. However, as the particle size distribution broadens, the deviation increases with increasing time on stream. This pronounced deviation partly explains the discrepancies between the particle size diameter derived from CO chemisorption and the STEM data. In addition, Equation (1) assumes particles with a perfect hemispherical shape, which is only an approximation and therefore does not consider alternative particle morphologies or dynamic changes during the aging. However, since such phenomena are of high relevance, especially for the bimetallic samples, the following section shines a light on morphological aspects.

2.2. Particle Morphology

Energy dispersive X-ray spectroscopy (EDXS) provided comprehensive information on the bimetallic catalyst samples, which is particularly relevant for investigating the degree of alloying and segregation. In the fresh state, the majority of bimetallic particles consisted of approximately 70% platinum and 30% palladium, which meets the target composition of a Pt:Pd weight ratio of 2:1 rather well. Figure 3a points to a minor tendency toward Pt-rich particles with increasing particle size, whereas the Pd content is slightly increased for smaller particles. While in this context platinum was always alloyed with palladium, some very small and highly dispersed monometallic palladium particles (<1 nm) were found throughout the fresh sample. Limitations with respect to the detector sensitivity that would avert detecting very small amounts of Pt within very small Pd particles are highly unlikely and the fact that the catalyst's target composition is Pt:Pd = 2:1, and the bimetallic particles found show only about 30% Pd instead of approximately 33%, strongly suggests the presence of monometallic species. Hence, we attribute the comparably high dispersion of the fresh Pt-Pd/Al$_2$O$_3$ catalyst that was found by CO chemisorption (Figure 1, Table 1) to these highly dispersed particles. As discussed above, the first hour of aging causes the most pronounced particle size increase, suggesting that the finely dispersed palladium particles disappear, either by formation of very palladium-rich particles or by embedding into the bimetallic Pt-Pd nanoparticles. Figure 3b provides clear evidence for the latter hypothesis, since the real average composition of the particles meets the target composition rather well. While large particles (>15 nm) still indicate a minor tendency toward Pt-rich alloys after only one hour of aging, further hydrothermal treatment seems to homogenize the overall elemental composition of the bimetallic particles (Figure 3c). However, a thorough in-depth analysis of the obtained energy dispersive X-ray spectroscopy (EDXS) images provides even more details.
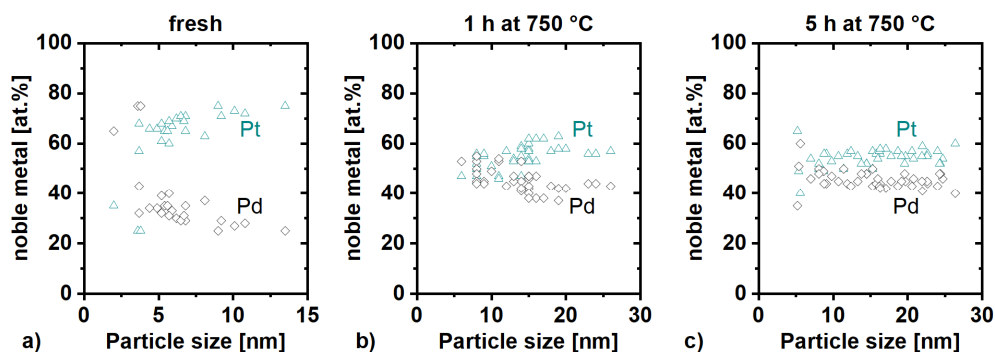
Figure 3. Noble metal distribution of bimetallic Pt-Pd particles in the fresh state (**a**), after aging for 1 h at 750 °C (**b**) and after aging for 5 h at 750 °C (**c**).

Notably, the bimetallic alloyed particles mostly showed homogeneously distributed Pt-Pd in the fresh state (Figure 4a). However, in several cases also a core-shell-like distribution was found (Figure A1a). In these structures, a palladium-rich alloy forms a shell and a platinum-rich alloy was mainly found in the core of the bimetallic particle. The lower surface tension of palladium oxide that was previously reported in fundamental investigations [36,37] may explain this trend and will be thoroughly discussed in the following section. After only one hour of hydrothermal aging, the number of such core-shell particles increased significantly. Also their overall composition changed slightly, essentially meeting the target Pt:Pd composition of 2:1 (Figure 3b). As no more highly dispersed (monometallic) species were found after hydrothermal aging, the aging causes an integration of the very small mobile Pd particles into larger ones. This enrichment of bimetallic alloys with palladium occurred in both, the platinum-rich core and the palladium-rich shell (Figure 4b). Although core-shell particles were still present and the particle composition did not show noteworthy changes, further hydrothermal treatment (5 h) induced formation of palladium-rich "islands" on the particles' outer rim, as shown in Figure 4c. This trend continues with time on stream, ultimately leading to a pronounced separation of the noble metal after 16 h of hydrothermal aging at 750 °C (Figure 4d). The majority of particles exhibited an inhomogeneous distribution of palladium and platinum, which points to a segregation of the noble metals. EDXS line scans as shown in Figure 5 clearly indicate a de-alloying and formation of inhomogeneous particles. Although the EDXS data do not allow to distinguish, whether this separation exclusively happens on the palladium-rich surface, or also in the platinum-rich core of the bimetallic particles, these information can help understanding the deactivation phenomena of bimetallic Pt-Pd diesel oxidation catalysts, which are presented in the following section.
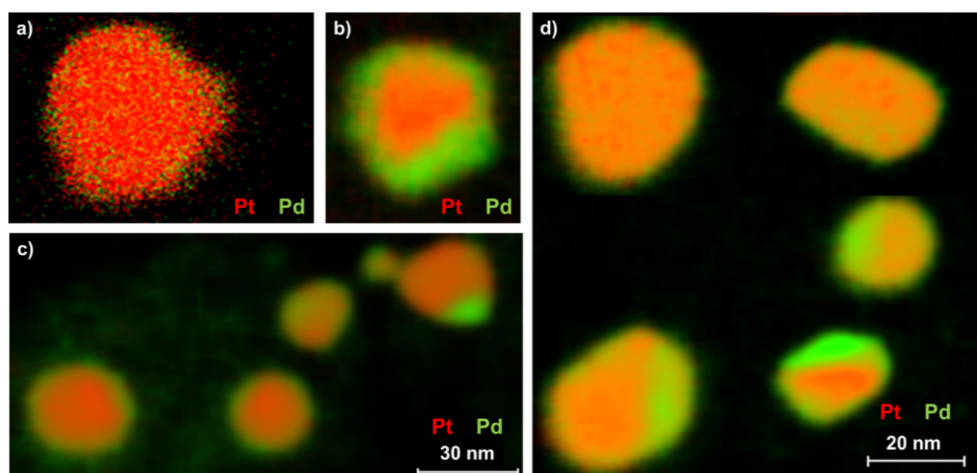
Figure 4. Energy dispersive X-ray spectroscopy (EDXS) scan of Pt-Pd particles in the fresh state (**a**) and after aging for 1 h at 750 °C (**b**), 5 h at 750 °C (**c**) and 16 h at 750 °C (**d**).
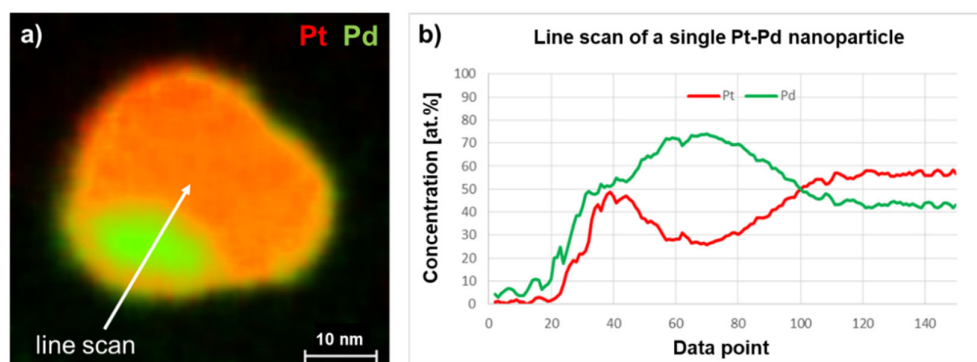

Figure 5. Representative EDXS line scan of a single Pt-Pd particle after aging for 16 h at 750 °C with an overview on the elemental composition of the bimetallic particle (**a**) and the detailed elemental concentrations along the line scan (**b**).

2.3. Catalytic Activity Measurements

Light-off measurements after an either reductive or oxidative pretreatment were conducted in order to evaluate the catalytic activity at several aging states. For this, the catalyst was heated with a ramp rate of 3 K/min from 60 °C to 180 °C in a gas mixture of 800 ppm CO, 7% CO_2, 5% O_2, 5% H_2O and balance N_2 (GHSV = 80 000 h^{-1}) while monitoring the CO conversion. Figure 6 summarizes the CO light-off activity of all catalyst samples after reduction prior to the activity test. In the fresh catalyst state we observed the highest CO oxidation activity for prereduced Pt-Pd/Al_2O_3, exhibiting a T_{50} (temperature of 50% conversion) of 103 °C, whereas T_{50} was 111 °C for Pd/Al_2O_3 and 127 °C for Pt/Al_2O_3. Irrespective of the catalyst formulation, the first hour of hydrothermal aging caused the most pronounced deactivation (Figure 6) for all samples, resulting in a T_{50} of 162 °C for Pt/Al_2O_3, 129 °C for Pd/Al_2O_3, and 136 °C for Pt-Pd/Al_2O_3. Hence, the bimetallic Pt-Pd/Al_2O_3 catalyst benefits from Pd addition as it shows less deactivation after one hour of aging than the monometallic Pt/Al_2O_3 sample. This trend is also valid after 5 h and 16 h of aging, respectively, ultimately resulting in a T_{50} of 170 °C for Pt/Al_2O_3 and 143 °C for Pt-Pd/Al_2O_3. With an aging-induced shift of T_{50} by 27 °C towards higher temperatures, monometallic Pd/Al_2O_3 exhibits the least pronounced deactivation after 16 h of hydrothermal treatment, which underscores the high thermal stability of Pd-based catalysts that was reported in the past [32,33]. This ΔT_{50} is 40 °C for the Pt-Pd catalyst and 43 °C for the Pt-

catalyst, respectively. Hence, the palladium addition predominantly benefits the bimetallic catalyst in the fresh state, whereas this beneficial activity boost is lost with longer aging periods.
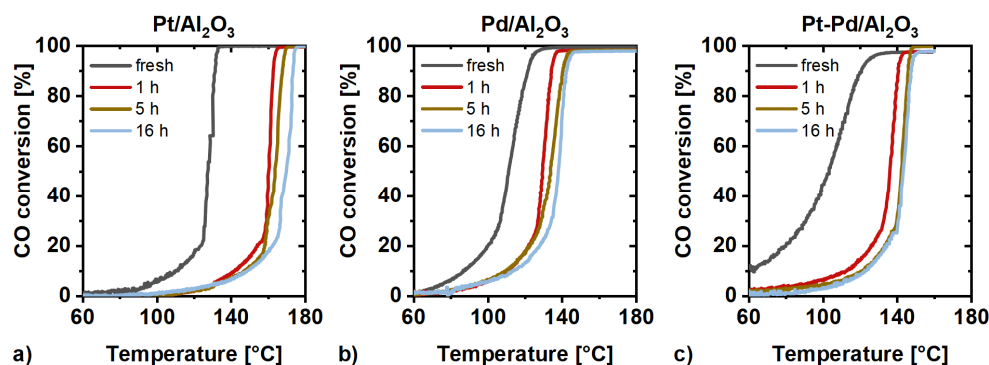

Figure 6. Catalytic activity for CO conversion of reduced Pt/Al_2O_3 (**a**), Pd/Al_2O_3 (**b**), and Pt-Pd/Al_2O_3 (**c**) during a light-off test in 800 ppm CO, 7% CO_2, 5% O_2, 5% H_2O, and bal. N_2 at a gas hourly space velocity (GHSV) of 80 000 h^{-1}.

The catalyst samples that were oxidized prior to the light-off showed an analogous behavior with respect to CO conversion and exhibited only minor differences in the overall activity trends (Figure A2). Nevertheless, monometallic Pt samples that were reduced prior to the light-off test showed slightly higher activity, both in the fresh state and after aging. This is in line with previous research that identified metallic platinum as most active for oxidation reactions [15,16]. Notably, an oxidative pretreatment at 400 °C slightly enhanced the catalytic activity of Pd/Al_2O_3 compared to the reduced catalyst sample and decreased T_{50} by approximately 5 to 10 °C (Figure A3). Since this beneficial effect was less pronounced for the bimetallic sample, we can conclude that the behavior of Pt-Pd/Al_2O_3 is dominated by platinum.

With a continuous decrease of the NO conversion after each aging step, the NO light-off measurements also confirmed a continuous catalyst deactivation with time on stream (Figure 7, Figure A4). The reduced Pt/Al_2O_3 sample exhibits a T_{50} of 179 °C, which increases during the stepwise aging to 190 °C after 1 h, to 209 °C after 5 h and to 236 °C after 16 h (Figure 7a). Over Pd/Al_2O_3 only negligible NO conversion was found (Figure A5), which explains the significantly lower NO oxidation activity of Pt-Pd/Al_2O_3 compared to the monometallic platinum catalyst. As depicted in Figure 7b, Pt-Pd/Al_2O_3 achieved 50% of NO conversion only in the fresh state. Oxidative treatment prior to the light-off resulted in slightly higher activity and allows for up to 58% NO conversion after 1 h of aging, up to 57% after 5 h of aging and up to 55% after 16 h of aging. Overall, we can conclude that despite the slight differences caused by the either reductive or oxidative pretreatment, the overall trend of declining activity after several aging iterations remains unchanged.
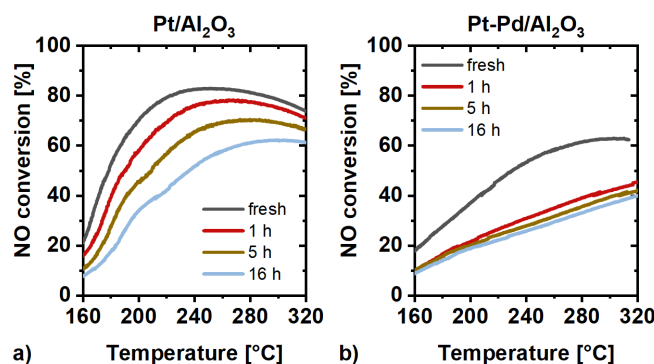
Figure 7. Catalytic activity for NO conversion after reductive pretreatment of Pt/Al₂O₃ (**a**) and Pt-Pd/Al₂O₃ (**b**) during a light-off test in 800 ppm NO, 7% CO₂, 5% O₂, 5% H₂O, and bal. N₂ at a GHSV of 40 000 h⁻¹.

3. Discussion

EDXS analysis of fresh and aged Pt-Pd/Al₂O₃ catalysts clearly revealed gradual morphological changes of the bimetallic samples, which were induced by hydrothermal aging in 400 ppm CO, 100 ppm C₃H₆, 7% CO, 12% O₂, 10% H₂O and balance N₂ at 750 °C. In the fresh catalyst state, the majority of particles consists of homogeneous bimetallic alloys and only in some cases core-shell-like structures with a palladium-rich shell and a platinum-rich core were found. These few core-shell particles could originate from the preconditioning that was conducted prior to our investigations (24 h in air, GHSV = 10 000 h⁻¹ at 550 °C, cf. Section 5.3.). In addition, small palladium particles with an almost atomic dispersion were found in the fresh state. Aging substantially increased the number of core-shell particles and caused continuous de-alloying and separation of the noble metals. This confirms earlier findings by Morlang et al. [29], who also found indications for Pt enrichment in the interior of particles after hydrothermal treatment of Pt-Pd catalysts. As shown in Section 2.2, the noble metal separation culminates in formation of platinum-rich particles that seem to have palladium-rich areas on their outer surface after 16 h of catalyst aging. In this state, the particles resemble segregated platinum and palladium structures rather than core-shell particles. These remarkable morphological changes of the alloy are accompanied by a continuous increase of the particle size that finally leads to an approximately four times higher mean particle size than in the fresh state. The pronounced sintering especially after the first hour can be attributed to Ostwald-ripening [50], as the nearly atomically dispersed palladium particles that EDXS uncovered in the fresh state disappear during the hydrothermal treatment. Although the subsequent aging steps cause further sintering (Table 1), the loss of dispersion declines and seems to converge in a stable catalyst state (Figure 1). This trend was analogously observed for the monometallic catalyst samples. According to Hansen et al. [50], particle migration and coalescence becomes a relevant aging mechanism during the subsequent aging steps and results in further but slower sintering. With increasing particle size, the relevance of surface tension effects [31–33,37] rises, which particularly influences the Pt-Pd alloy. Moreover, compared to metallic Pt, Galeev et al. [53] report a lower surface energy for metallic palladium. Such energy differences result in a different stability of the noble metal phases and can ultimately promote a separation of palladium and platinum. Under reaction conditions, also the highly complex and vigorously debated dynamic Pd-PdO transformation [54–56] may contribute to weakening interactions between the two noble metal phases, since dynamic changes in the crystallite lattice can result in particle size changes and surface roughening. Finally yet importantly, not only the oxygen content of the palladium phase, but also its localization, precisely surface palladium oxide, bulk palladium oxide, or subsurface oxide, has been identified as a major factor for high CO conversion [57]. Hence, a variety of concurrent effects can tremendously affect the catalyst's behavior.

As revealed by means of CO chemisorption, the pronounced particle growth that we observed in the STEM images causes a decreasing availability of catalytically active surface sites. Since the number of active sites is a key driver for the catalytic activity of noble metal particles [58], their decrease results in a pronounced activity loss, as observed during consecutive CO and NO light-off measurements. Compared to the monometallic Pt/Al_2O_3 catalyst, the bimetallic $Pt-Pd/Al_2O_3$ catalyst strongly benefits from palladium addition with respect to the catalytic CO oxidation activity (Figure 6). This also becomes obvious for the turnover frequency (TOF; Figure A6). In the fresh state, we found decreasing TOFs that follow the trend Pd > Pt-Pd > Pt. Interestingly, the TOF for the bimetallic catalyst drops below the monometallic Pt catalyst after 16 h of aging, although the catalytic conversion remains comparatively high. During the light-off test, for instance, $Pt-Pd/Al_2O_3$ showed full CO conversion at 160 °C in each aging state, whereas under the same conditions Pt/Al_2O_3 converted only 18% of CO after 16 h of hydrothermal aging. Since the TOF was calculated based on dispersion values obtained from CO chemisorption measurements, morphological changes cannot be considered. However, our results clearly reveal simultaneous changes of morphology, particle size, and degree of alloying. Deconvolution of such simultaneous effects requires extremely well defined catalyst samples and advanced in situ techniques, which is beyond the scope of the present study. Therefore, we can only speculate that the higher dispersion of the bimetallic catalyst sample ensures a high activity, although the efficiency of the active sites in the bimetallic sample is lower, possibly due to the noble metal separation.

Nevertheless, the activity trends suggest attributing the high CO oxidation activity of $Pt-Pd/Al_2O_3$ to the Pd species. With longer aging time and advancing noble metal separation and segregation, the role of palladium becomes progressively dominant. Consequently, the NO conversion strongly decreases after aging, because palladium only exhibits negligible NO oxidation activity. Coverage of the platinum-rich particles with highly palladium-rich phases hinders access of NO to the active Pt sites and results in an NO oxidation activity drop. This is in line with previous work by Graham and co-workers [34], who underscored the crucial role of platinum surface species that need to be accessible for the NO molecules. Overall, we can conclude that the hydrothermal aging of the bimetallic $Pt-Pd/Al_2O_3$ catalyst causes twofold deactivation with respect to CO and NO oxidation activity. The number of catalytically active surface sites decreases with time on stream and at the same time also de-alloying occurs.

4. Conclusions

Although both sintering and separation of the noble metals progresses with time on stream, we cannot derive a clear correlation between particle size and morphology. The very Pd-rich islands on the Pt-rich particles seem to have a random distribution. Since we analyzed a sufficient number of representative particles for each catalyst sample, we assume that this cannot be attributed to statistical spreading. Therefore, we conclude that the catalytic activity does not only decline due to a decreasing number of catalytically active surface sites, but also due to the loss of the beneficial properties of the bimetallic alloy particles. In our study, we investigated model catalysts that were coated onto a cordierite substrate and that were treated under industrially relevant conditions. However, more detailed insights are highly desirable, particularly when aiming at resilient structure-activity correlations. EDXS elemental analysis, as used in this study, allows only an integral view from top to bottom, averaging elemental concentrations through the entire particle. However, a precise three-dimensional analysis of the spatial distribution of both noble metals is not possible. Therefore, the exact position of the palladium-rich islands that we observed around the platinum-rich particles after aging remains unclear. Moreover, migration to the washcoat bulk may also occur, which could further decrease the catalytic activity. In this respect, tomographic investigations, e.g., as suggested by Sheppard et al. [59], offer a powerful alternative technique for obtaining further fundamental insights in the future.

The results presented in this paper are of high relevance for the design of bimetallic catalysts in the future. Particularly in the context of diesel oxidation catalysts, ceria has been in the focus of scientific interest in the past years, since it can tremendously influence the catalytic activity due to its strong noble metal support interactions [22,60,61]. In the context of a CeO$_x$/Pt(111) inverse model catalyst, Suchorski et al. [62], for instance, proposed an "active border" between CeO$_x$ and Pt as reason for enhanced catalytic activity. However, previous findings indicate that these interactions, namely the high attraction between Pt and CeO$_2$ [60], may cause a separation of the noble metals in bimetallic Pt-Pd catalysts supported on ceria-containing support materials [63]. Therefore, it will be interesting to expand the fundamental investigations discussed in our present study into bimetallic catalyst samples with alternative support materials. Preferably, such investigations should be conducted with well-defined catalyst structures that allow for systematically investigating different effects like crystallite size and noble metal support interactions on the catalytic behavior [21]. Deconvolution of simultaneous effects is a particularly crucial factor for understanding and improving state-of-the-art catalyst systems. In this respect, even longer aging periods may be considered, as structural changes of the support material typically require either longer aging periods or more severe aging conditions [50,64]. Such investigations will add more facets to the profound knowledge on the aging-induced changes of bimetallic noble metal particles as subject to our study and can help improving catalysts in the future. Ultimately, this will ensure maximum long-time exploitation of the noble metal, hereby offering the chance to reduce the overall costs of catalytic converters.

5. Materials and Methods

5.1. Catalyst Samples

For our present study, we investigated a series of non-commercial model catalyst samples provided by Umicore AG & Co. KG (Hanau, Germany). The washcoated cordierite honeycombs (400 cpsi, 6.5 mil) exhibited a noble metal loading of 80 g/ft^3, containing either Pt, Pd, or a mixture of Pt and Pd in a weight ratio of 2:1 on γ-Al$_2$O$_3$. For activity measurements and CO chemisorption measurements, monolithic samples with a length of 6 cm and a diameter of 2.54 cm were used. Their washcoat was mechanically removed from the cordierite substrate prior to characterization by scanning transmission electron microscopy (STEM) and energy dispersive X-ray spectroscopy (EDXS).

5.2. Catalyst Characterization

An aberration-corrected FEI Titan transmission electron microscope (FEI Company, Hillsboro, OR, USA) at 300 keV in scanning transmission electron microscopy (STEM) mode equipped with a high angle annular dark field (HAADF) detector provided information on the particle size and morphology of the noble metal particles. Furthermore, energy dispersive X-ray spectroscopy (EDXS) allowed analyzing bimetallic Pt-Pd particles with regard to elemental composition and alloying level. The elemental mapping was done with an FEI OSIRIS ChemiSTEM microscope (FEI Company, Hillsboro, OR, USA) at 200 keV and the obtained data were evaluated with the ESPRIT software package for micro- and nano-analysis (Bruker Corporation, Billerica, MA, USA). Platinum and palladium were quantified by using the Pt-Lα and Pd-Lα line, respectively, while the washcoat (Al, O), the TEM-Grid (C) and the sample holder (Cu) served as background.

The mean noble metal particle size obtained by evaluating several representative electron microscopy images was verified by means of CO chemisorption. This approach reveals the overall noble metal dispersion of the monolithic samples, which were also used for activity measurements. After placing these samples in a tubular quartz glass reactor (QSIL AG, Ilmenau, Germany), the catalysts were pretreated with air for 30 min at 550 °C and were subsequently reduced with 5% H$_2$ in N$_2$ at 400 °C for 60 min. After cooling

the reactor down to room temperature under continuous N_2 flow, the catalyst was saturated with 1% CO in N_2 for 60 min. Once the system was flushed again with N_2 in order to remove free and physisorbed CO, a temperature programmed desorption of CO (CO-TPD) was performed under inert N_2 gas flow by heating with a slope of 20 K/min to a maximum temperature of 550 °C. Gas concentrations of CO and CO_2 were monitored with an infrared (IR) detector (BINOS 1000, Fisher-Rosemount GmbH & Co, Hasselroth, Germany). For calculating the noble metal dispersion, an adsorption stoichiometry of 1:1 (CO:Pd and CO:Pt) was assumed [52].

5.3. Catalytic Tests

Activity measurements were executed in a laboratory test setup, which was controlled by an in-house developed LabView software that allows automated catalytic tests with high precision and reproducibility. Monolithic samples were placed in a cylindrical quartz glass sample holder in a plug-flow quartz tube reactor surrounded by an electrical furnace. Thermocouples (type N; d = 1 mm; TC Mess- und Regeltechnik GmbH, Mönchengladbach, Germany) that were located directly in front and after the sample and connected to Eurotherm controllers (Schneider Electric Systems Germany GmbH, Neuss, Germany) were used for temperature management and monitoring. Gases were dosed with mass flow controllers (MFCs; Bronkhorst Deutschland Nord GmbH, Kamen, Germany) via heated stainless steel lines. Notably, NO was dosed via a separate pipe almost directly in front of the sample in order to suppress the reaction from NO to NO_2 in the dosing line. Water vapor was provided using a controlled evaporation mixer (CEM; Bronkhorst, Deutschland Nord GmbH, Kamen, Germany). A Fourier-transform infrared (FTIR) analyzer (MultiGas 2030; MKS Instruments, Andover, MA, USA) and an O_2-analyzer (Magnos 16; Hartmann & Braun/ABB, Zürich, Switzerland) allow an on-line analysis of the gas composition.

Prior to activity tests and characterization, all samples were preconditioned at 550 °C for 24 h in air, with a GHSV of 10 000 h^{-1} (corresponds to 10.13 L min^{-1}; sample state: "fresh"). Light-off experiments were conducted in a gas atmosphere containing 7% CO_2, 5% O_2, 5% H_2O, balance N_2, and 800 ppm of either CO or NO (Table 2). While NO light-off measurements were performed at a GHSV of 40 000 h^{-1} (corresponds to 20.27 L min^{-1}), CO light-off measurements were performed at a GHSV of 80 000 h^{-1} (corresponds to 40.54 L min^{-1}) due to the fast reaction. For aging, the atmosphere was changed to get a more realistic model exhaust that does not only contain water, but also hydrocarbons (Table 2, "Hydrothermal aging"). Since previous experiments did not reveal a noteworthy influence of NO on the aging behavior of the catalyst samples (data not shown), the aging gas mixture did not contain NO. Light off measurements were done after a reductive pretreatment with 3% H_2 in N_2 at 350 °C for 60 min and cooling down in N_2. As illustrated in Figure 8, the CO light off experiments were executed by heating up from 80 °C to 180 °C with a slope of 3 K/min, further heating to 400 °C and holding for 30 min in oxidative conditions (same gas mixture as chosen for the CO light-off test). Cooling down in N_2 to 80 °C and performing a second run (heating to 180 °C with 3 K/min) allows a direct comparison between the catalytic activity after reductive and oxidative pretreatment. Similarly, the NO light off was executed by heating up from 160 °C to 320 °C with a slope of 3 K/min, followed by cooling down in N_2 to 80 °C and performance of a second run (heating to 320 °C with 3 K/min).

Table 2. Gas concentrations in vol.% used during the light-off measurements and during sample aging.

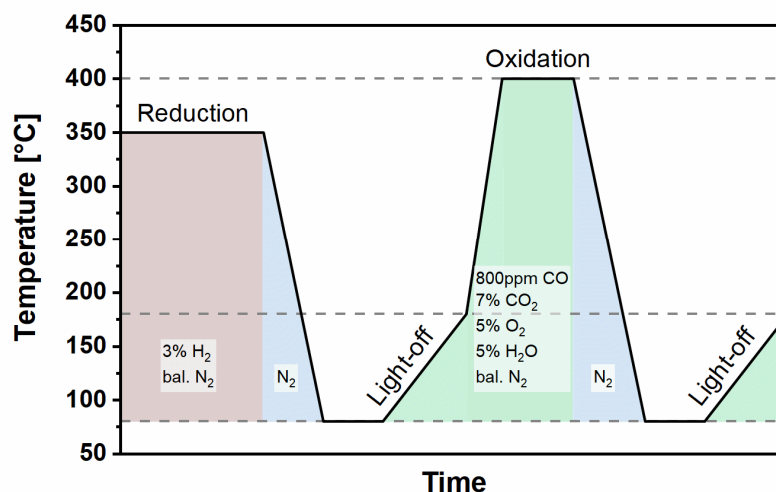|	CO	NO	C_3H_6	CO_2	O_2	H_2O	N_2	GHSV
CO light-off	0.08	-	-	7	5	5	Bal.	80 000 h^{-1}
NO light-off	-	0.08	-	7	5	5	Bal.	40 000 h^{-1}
Hydrothermal aging	0.04	-	0.01	7	12	10	Bal.	20 000 h^{-1}

Figure 8. Schematic overview on the experimental procedure during the CO light-off experiments.

Calculating the turnover frequency (TOF) allows comparing the catalysts among each other by taking their catalytic activity and the dispersion values obtained by CO chemisorption measurements into account. Equation (2) defines the TOF [s^{-1}] as

$$TOF = \frac{\dot{V} \cdot X \cdot c_0(CO) \cdot \frac{p}{R \cdot T}}{\frac{m_{noble\,metal}}{M_{noble\,metal}} \cdot D}, \qquad (2)$$

with $\dot{V}$ as the volumetric flow rate [$m^3\,s^{-1}$], X as the conversion ($0 \leq X \leq 1$), $c_0(CO)$ as volumetric inlet concentration of CO [ppmv], p as pressure [Pa], R as gas constant (R = 8.314 J K^{-1} mol^{-1}), T as temperature [K], $m_{noble\,metal}$ as mass of the noble metal on the monolithic sample [kg], $M_{noble\,metal}$ as the molar mass of the noble metal [kg mol^{-1}] and D as dispersion ($0 \leq D \leq 1$). Please note that for the bimetallic catalyst samples, the calculation according to Equation (2) includes the consideration of the Pt-Pd weight ratio of 2:1.
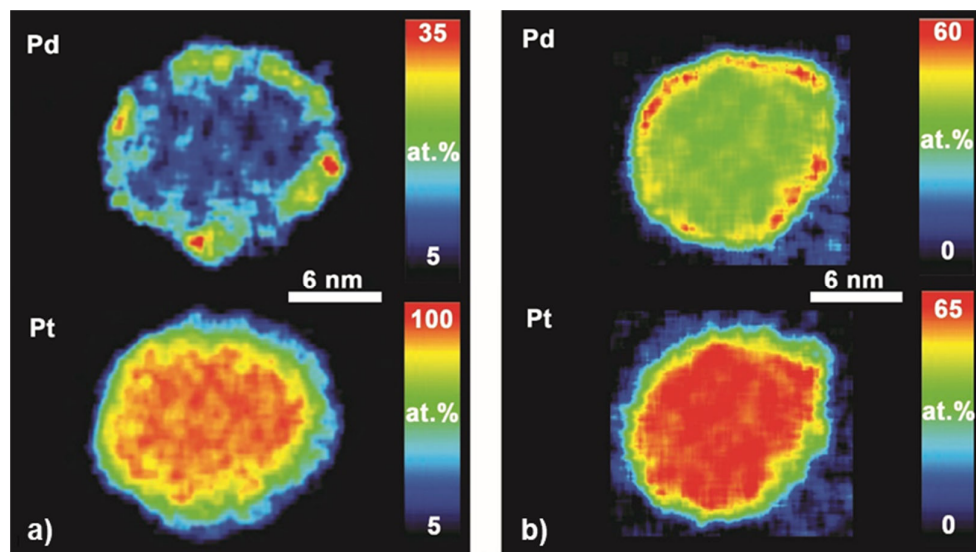
Appendix A

Figure A1. EDXS scan of Pt-Pd particles in the fresh state (**a**) and after aging for 1 h at 750 °C (**b**).
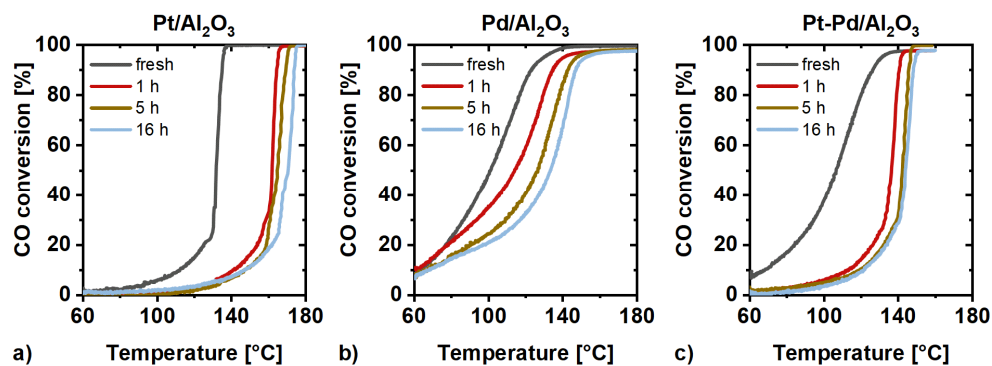
Figure A2. Catalytic activity for CO conversion after oxidative pretreatment of Pt/Al_2O_3 (**a**), Pd/Al_2O_3 (**b**), and $Pt-Pd/Al_2O_3$ (**c**) during a light-off test in 800 ppm CO, 7% CO_2, 5% O_2, 5% H_2O, and bal. N_2 at a GHSV of 80 000 h^{-1}.
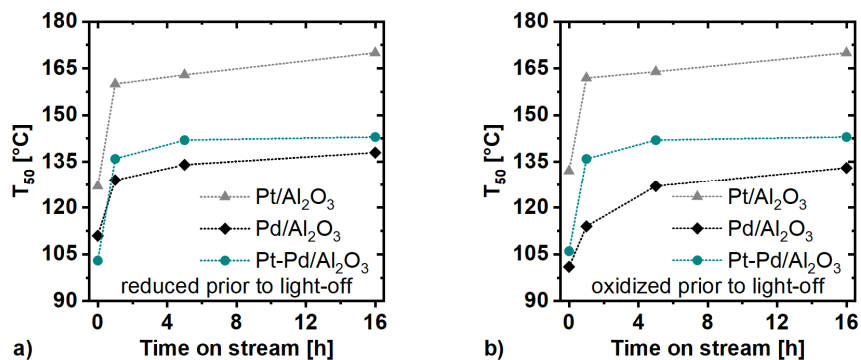

Figure A3. Temperature of 50% conversion (T_{50}) of CO during light off tests in 800 ppm CO, 7% CO_2, 5% O_2, 5% H_2O, and bal. N_2 at a GHSV of 80 000 h^{-1} of reduced (**a**) and oxidized (**b**) Pt/Al_2O_3, Pd/Al_2O_3, and $Pt-Pd/Al_2O_3$.
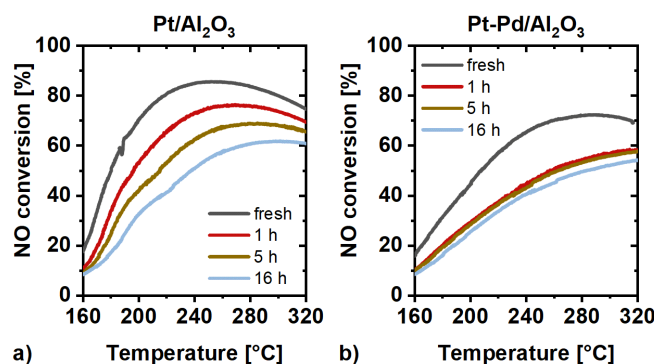
Figure A4. Catalytic activity for NO conversion after oxidative pretreatment of Pt/Al$_2$O$_3$ (**a**), and Pt-Pd/Al$_2$O$_3$ (**b**) during a light-off test in 800 ppm NO, 7% CO$_2$, 5% O$_2$, 5% H$_2$O, and bal. N$_2$ at a GHSV of 40 000 h^{-1}.
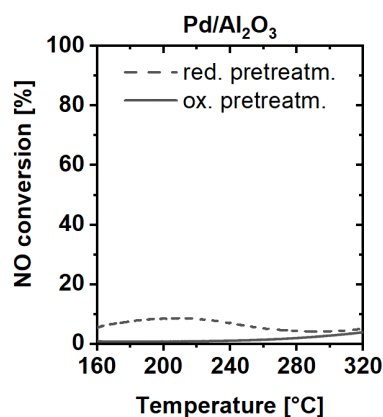

Figure A5. Catalytic activity for NO conversion after reductive and oxidative pretreatment of Pd/Al$_2$O$_3$ (fresh state) during a light-off test in 800 ppm NO, 7% CO$_2$, 5% O$_2$, 5% H$_2$O, and bal. N$_2$ at a GHSV of 40 000 h^{-1}.
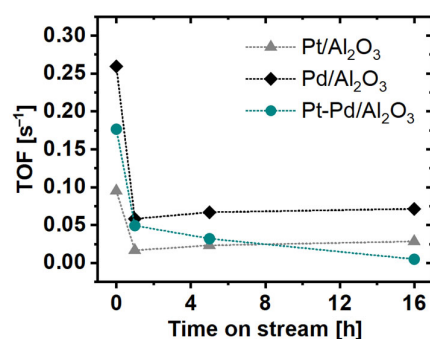
Figure A6. Turnover frequency (TOF) for CO oxidation at 120 °C of Pt/Al$_2$O$_3$, Pd/Al$_2$O$_3$ and Pt-Pd/Al$_2$O$_3$ during a light-off test (after reductive pretreatment) in 800 ppm CO, 7% CO$_2$, 5% O$_2$, 5% H$_2$O, and bal. N$_2$ at a GHSV of 80 000 h^{-1}.

References

1. Deutschmann, O.; Grunwaldt, J.-D. Exhaust Gas Aftertreatment in Mobile Systems: Status, Challenges, and Perspectives. *Chem. Eng. Tech.* **2013**, *85*, 595–617, doi:10.1002/cite.201200188.
2. Russell, A.; Epling, W.S. Diesel Oxidation Catalysts. *Catal. Rev.* **2011**, *53*, 337–423, doi:10.1080/01614940.2011.596429.
3. Johnson, T.V. Review of diesel emissions and control. *Int. J. Eng. Res.* **2009**, *10*, 275–285, doi:10.1243/14680874JER04009.

4. Johnson, T.V. Diesel Emission Control in Review. *SAE Int. J. Fuels Lubr.* **2009**, *1*, 68–81, doi:10.4271/2008-01-0069.

5. Mulla, S.; Chen, N.; Cumaranatunge, L.; Blau, G.; Zemlyanov, D.; Delgass, W.; Epling, W.S.; Ribeiro, F. Reaction of NO and O_2 to NO_2 on Pt: Kinetics and catalyst deactivation. *J. Catal.* **2006**, *241*, 389–399, doi:10.1016/j.jcat.2006.05.016.

6. Boubnov, A.; Dahl, S.; Johnson, E.; Molina, A.P.; Simonsen, S.B.; Cano, F.M.; Helveg, S.; Lemus-Yegres, L.J.; Grunwaldt, J.-D. Structure–activity relationships of Pt/Al_2O_3 catalysts for CO and NO oxidation at diesel exhaust conditions. *Appl. Catal. B* **2012**, *126*, 315–325, doi:10.1016/j.apcatb.2012.07.029.

7. Lira, E.; Merte, L.R.; Behafarid, F.; Ono, L.K.; Zhang, L.; Roldan Cuenya, B. Role and Evolution of Nanoparticle Structure and Chemical State during the Oxidation of NO over Size- and Shape-Controlled $Pt/\gamma-Al_2O_3$ Catalysts under Operando Conditions. *ACS Catal.* **2014**, *4*, 1875–1884, doi:10.1021/cs500137r.

8. Hansen, T.K.; Høj, M.; Hansen, B.B.; Janssens, T.V.W.; Jensen, A.D. The Effect of Pt Particle Size on the Oxidation of CO, C_3H_6, and NO Over Pt/Al_2O_3 for Diesel Exhaust Aftertreatment. *Top. Catal.* **2017**, *60*, 1333–1344, doi:10.1007/s11244-017-0818-9.

9. Lee, J.-H.; Kung, H.H. Effect of Pt dispersion on the reduction of NO by propene over alumina-supported Pt catalysts under lean-burn conditions. *Catal. Lett.* **1998**, *51*, 1–4, doi:10.1023/A:1019068530266.

10. Auvray, X.; Pingel, T.; Olsson, E.; Olsson, L. The effect gas composition during thermal aging on the dispersion and NO oxidation activity over Pt/Al_2O_3 catalysts. *Appl. Catal. B* **2013**, *129*, 517–527, doi:10.1016/j.apcatb.2012.10.002.

11. Johns, T.R.; Gaudet, J.R.; Peterson, E.J.; Miller, J.T.; Stach, E.A.; Kim, C.H.; Balogh, M.P.; Datye, A.K. Microstructure of Bimetallic Pt-Pd Catalysts under Oxidizing Conditions. *ChemCatChem* **2013**, *5*, 2636–2645, doi:10.1002/cctc.201300181.

12. Ogel, E.; Casapu, M.; Doronkin, D.E.; Popescu, R.; Störmer, H.; Mechler, C.; Marzun, G.; Barcikowski, S.; Türk, M.; Grunwaldt, J.-D. Impact of Preparation Method and Hydrothermal Aging on Particle Size Distribution of $Pt/\gamma-Al_2O_3$ and Its Performance in CO and NO Oxidation. *J. Phys. Chem. C* **2019**, *123*, 5433–5446, doi:10.1021/acs.jpcc.8b11065.

13. Casapu, M.; Fischer, A.; Gänzler, A.M.; Popescu, R.; Crone, M.; Gerthsen, D.; Türk, M.; Grunwaldt, J.-D. Origin of the Normal and Inverse Hysteresis Behavior during CO Oxidation over Pt/Al_2O_3. *ACS Catal.* **2016**, *7*, 343–355, doi:10.1021/acscatal.6b02709.

14. Hauff, K.; Tuttlies, U.; Eigenberger, G.; Nieken, U. Platinum oxide formation and reduction during NO oxidation on a diesel oxidation catalyst—Experimental results. *Appl. Catal. B* **2012**, *123–124*, 107–116, doi:10.1016/j.apcatb.2012.04.008.

15. Gänzler, A.M.; Casapu, M.; Boubnov, A.; Müller, O.; Conrad, S.; Lichtenberg, H.; Frahm, R.; Grunwaldt, J.-D. Operando spatially and time-resolved X-ray absorption spectroscopy and infrared thermography during oscillatory CO oxidation. *J. Catal.* **2015**, *328*, 216–224, doi:10.1016/j.jcat.2015.01.002.

16. Boubnov, A.; Gänzler, A.M.; Conrad, S.; Casapu, M.; Grunwaldt, J.-D. Oscillatory CO Oxidation Over Pt/Al_2O_3 Catalysts Studied by In situ XAS and DRIFTS. *Top. Catal.* **2013**, *56*, 333–338, doi:10.1007/s11244-013-9976-6.

17. Dubbe, H.; Eigenberger, G.; Nieken, U. Modeling of Conversion Hysteresis Phenomena for Pt/Pd-based Diesel Oxidation Catalysts. *Chem. Eng. Tech.* **2018**, *90*, 625–633, doi:10.1002/cite.201700134.

18. Hauff, K.; Dubbe, H.; Tuttlies, U.; Eigenberger, G.; Nieken, U. Platinum oxide formation and reduction during NO oxidation on a diesel oxidation catalyst—Macrokinetic simulation. *Appl. Catal. B* **2013**, *129*, 273–281, doi:10.1016/j.apcatb.2012.09.022.

19. Olsson, L.; Fridell, E. The Influence of Pt Oxide Formation and Pt Dispersion on the Reactions $NO_2 \Leftrightarrow NO + 1/2\ O_2$ over Pt/Al_2O_3 and $Pt/BaO/Al_2O_3$. *J. Catal.* **2002**, *210*, 340–353, doi:10.1006/jcat.2002.3698.

20. Gänzler, A.M.; Casapu, M.; Doronkin, D.E.; Maurer, F.; Lott, P.; Glatzel, P.; Votsmeier, M.; Deutschmann, O.; Grunwaldt, J.-D. Unravelling the Different Reaction Pathways for Low Temperature CO Oxidation on Pt/CeO_2 and Pt/Al_2O_3 by Spatially Resolved Structure-Activity Correlations. *J. Phys. Chem. Lett.* **2019**, *10*, 7698–7705, doi:10.1021/acs.jpclett.9b02768.

21. Cargnello, M.; Doan-Nguyen, V.V.T.; Gordon, T.R.; Diaz, R.E.; Stach, E.A.; Gorte, R.J.; Fornasiero, P.; Murray, C.B. Control of metal nanocrystal size reveals metal-support interface role for ceria catalysts. *Science* **2013**, *341*, 771–773, doi:10.1126/science.1240148.

22. Gänzler, A.M.; Casapu, M.; Vernoux, P.; Loridant, S.; Cadete Santos Aires, F.J.; Epicier, T.; Betz, B.; Hoyer, R.; Grunwaldt, J.-D. Tuning the Structure of Platinum Particles on Ceria In Situ for Enhancing the Catalytic Performance of Exhaust Gas Catalysts. *Angew. Chem., Int. Ed.* **2017**, *56*, 13078–13082, doi:10.1002/anie.201707842.

23. Datye, A.K.; Votsmeier, M. Opportunities and challenges in the development of advanced materials for emission control catalysts. *Nat. Mater.* **2020**, doi:10.1038/s41563-020-00805-3.

24. Cao, A.; Lu, R.; Veser, G. Stabilizing metal nanoparticles for heterogeneous catalysis. *Phys. Chem. Chem. Phys.* **2010**, *12*, 13499–13510, doi:10.1039/c0cp00729c.

25. Wong, A.P.; Kyriakidou, E.A.; Toops, T.J.; Regalbuto, J.R. The catalytic behavior of precisely synthesized Pt–Pd bimetallic catalysts for use as diesel oxidation catalysts. *Catal. Today* **2016**, *267*, 145–156, doi:10.1016/j.cattod.2016.02.011.

26. Etheridge, J.E.; Watling, T.C.; Izzard, A.J.; Paterson, M.A.J. The Effect of Pt:Pd Ratio on Light-Duty Diesel Oxidation Catalyst Performance: An Experimental and Modelling Study. *SAE Int. J. Engines* **2015**, *8*, 1283–1299, doi:10.4271/2015-01-1053.

27. Kim, C.H.; Schmid, M.; Schmieg, S.J.; Tan, J.; Li, W. The Effect of Pt-Pd Ratio on Oxidation Catalysts Under Simulated Diesel Exhaust. *SAE Tech. Paper* **2011**, doi:10.4271/2011-01-1134.

28. Kaneeda, M.; Iizuka, H.; Hiratsuka, T.; Shinotsuka, N.; Arai, M. Improvement of thermal stability of NO oxidation $Pt/Al2O3$ catalyst by addition of Pd. *Appl. Catal. B* **2009**, *90*, 564–569, doi:10.1016/j.apcatb.2009.04.011.

29. Morlang, A.; Neuhausen, U.; Klementiev, K.V.; Schütze, F.-W.; Miehe, G.; Fuess, H.; Lox, E.S. Bimetallic Pt/Pd diesel oxidation catalysts: Structural characterisation and catalytic behaviour. *Appl. Catal. B* **2005**, *60*, 191–199, doi:10.1016/j.apcatb.2005.03.007.

30. Johns, T.R.; Goeke, R.S.; Ashbacher, V.; Thüne, P.C.; Niemantsverdriet, J.W.; Kiefer, B.; Kim, C.H.; Balogh, M.P.; Datye, A.K. Relating adatom emission to improved durability of Pt–Pd diesel oxidation catalysts. *J. Catal.* **2015**, *328*, 151–164, doi:10.1016/j.jcat.2015.03.016.

31. Plessow, P.N.; Abild-Pedersen, F. Sintering of Pt Nanoparticles via Volatile PtO_2. *ACS Catal.* **2016**, *6*, 7098–7108, doi:10.1021/acscatal.6b01646.

32. Alcock, C.B.; Hooper, G.W. Thermodynamics of the gaseous oxides of the platinum-group metals. *Proc. R. Soc. Lond. A* **1960**, *254*, 551–561, doi:10.1098/rspa.1960.0040.

33. Peuckert, M. XPS study on surface and bulk palladium oxide, its thermal stability, and a comparison with other noble metal oxides. *J. Phys. Chem.* **1985**, *89*, 2481–2486, doi:10.1021/j100258a012.

34. Graham, G.W.; Jen, H.-W.; Ezekoye, O.; Kudla, R.J.; Chun, W.; Pan, X.Q.; McCabe, R.W. Effect of alloy composition on dispersion stability and catalytic activity for NO oxidation over alumina-supported Pt–Pd catalysts. *Catal. Lett.* **2007**, *116*, 1–8, doi:10.1007/s10562-007-9124-7.

35. Neyestanaki, A.K.; Klingstedt, F.; Salmi, T.; Murzin, D.Y. Deactivation of postcombustion catalysts, a review. *Fuel* **2004**, *83*, 395–408, doi:10.1016/j.fuel.2003.09.002.

36. Ciuparu, D.; Pfefferle, L. Methane combustion activity of supported palladium catalysts after partial reduction. *Appl. Catal. A* **2001**, *218*, 197–209, doi:10.1016/S0926-860X(01)00643-3.

37. Ruckenstein, E.; Chen, J.J. Spreading and surface tension gradient driven phenomena during heating of alumina-supported palladium crystallites in oxygen. *J. Catal.* **1981**, *70*, 233–236, doi:10.1016/0021-9517(81)90334-1.

38. Carrillo, C.; Johns, T.R.; Xiong, H.; DeLaRiva, A.; Challa, S.R.; Goeke, R.S.; Artyushkova, K.; Li, W.; Kim, C.H.; Datye, A.K. Trapping of Mobile Pt Species by PdO Nanoparticles under Oxidizing Conditions. *J. Phys. Chem. Lett.* **2014**, *5*, 2089–2093, doi:10.1021/jz5009483.

39. Arnal, P.M.; Comotti, M.; Schüth, F. High-temperature-stable catalysts by hollow sphere encapsulation. *Angew. Chem., Int. Ed.* **2006**, *45*, 8224–8227, doi:10.1002/anie.200603507.

40. Hill, A.J.; Seo, C.Y.; Chen, X.; Bhat, A.; Fisher, G.B.; Lenert, A.; Schwank, J.W. Thermally Induced Restructuring of Pd@CeO₂ and Pd@SiO₂ Nanoparticles as a Strategy for Enhancing Low-Temperature Catalytic Activity. *ACS Catal.* **2020**, *10*, 1731–1741, doi:10.1021/acscatal.9b05224.

41. Cai, Y.; Xu, J.; Guo, Y.; Liu, J. Ultrathin, Polycrystalline, Two-Dimensional Co₃O₄ for Low-Temperature CO Oxidation. *ACS Catal.* **2019**, *9*, 2558–2567, doi:10.1021/acscatal.8b04064.

42. Yang, X.; Li, Q.; Lu, E.; Wang, Z.; Gong, X.; Yu, Z.; Guo, Y.; Wang, L.; Guo, Y.; Zhan, W.; et al. Taming the stability of Pd active phases through a compartmentalizing strategy toward nanostructured catalyst supports. *Nat. Commun.* **2019**, *10*, 1611, doi:10.1038/s41467-019-09662-4.

43. Malamis, S.A.; Harold, M.P.; Epling, W.S. Coupled NO and C₃H₆ Trapping, Release and Conversion on Pd/BEA: Evaluation of the Lean Hydrocarbon NOx Trap. *Ind. Eng. Chem. Res.* **2019**, *58*, 22912–22923, doi:10.1021/acs.iecr.9b04919.

44. Zheng, Y.; Kovarik, L.; Engelhard, M.H.; Wang, Y.; Wang, Y.; Gao, F.; Szanyi, J. Low-Temperature Pd/Zeolite Passive NOx Adsorbers: Structure, Performance, and Adsorption Chemistry. *J. Phys. Chem. C* **2017**, *121*, 15793–15803, doi:10.1021/acs.jpcc.7b04312.

45. Theis, J.R. An assessment of Pt and Pd model catalysts for low temperature NO adsorption. *Catal. Today* **2016**, *267*, 93–109, doi:10.1016/j.cattod.2016.01.032.

46. Günter, T.; Pesek, J.; Schäfer, K.; Bertótiné Abai, A.; Casapu, M.; Deutschmann, O.; Grunwaldt, J.-D. Cu-SSZ-13 as pre-turbine NOx-removal-catalyst: Impact of pressure and catalyst poisons. *Appl. Catal. B* **2016**, *198*, 548–557, doi:10.1016/j.apcatb.2016.06.005.

47. Xu, Q.; Kharas, K.C.; Croley, B.J.; Datye, A.K. The Sintering of Supported Pd Automotive Catalysts. *ChemCatChem* **2011**, *3*, 1004–1014, doi:10.1002/cctc.201000392.

48. McCarty, J.G.; Malukhin, G.; Poojary, D.M.; Datye, A.K.; Xu, Q. Thermal coarsening of supported palladium combustion catalysts. *J. Phys. Chem. B* **2005**, *109*, 2387–2391, doi:10.1021/jp048822w.

49. Fuentes, G.A.; Salinas-Rodríguez, E. Realistic Particle Size Distributions during Sintering by Ostwald Ripening. *Stud. Surf. Sci. Catal.* **2001**, *139*, 503–510, doi:10.1016/s0167-2991(01)80236-6.

50. Hansen, T.W.; Delariva, A.T.; Challa, S.R.; Datye, A.K. Sintering of catalytic nanoparticles: Particle migration or Ostwald ripening? *Acc. Chem. Res.* **2013**, *46*, 1720–1730, doi:10.1021/ar3002427.

51. Ruckenstein, E.; Pulvermacher, B. Kinetics of crystallite sintering during heat treatment of supported metal catalysts. *AIChE J.* **1973**, *19*, 356–364, doi:10.1002/aic.690190222.

52. Bergeret, G.; Gallezot, P. Particle Size and Dispersion Measurements. In *Handbook of Heterogeneous Catalysis*, 2nd ed.; Ertl, G., Ed.; Wiley-VCH: Weinheim, Germany; Chichester, UK, 2008; ISBN 9783527610044.

53. Galeev, T.K.; Bulgakov, N.N.; Savelieva, G.A.; Popova, N.M. Surface properties of platinum and palladium. *React. Kinet. Catal. Lett.* **1980**, *14*, 61–65, doi:10.1007/BF02061265.

54. Lott, P.; Dolcet, P.; Casapu, M.; Grunwaldt, J.-D.; Deutschmann, O. The Effect of Prereduction on the Performance of Pd/Al₂O₃ and Pd/CeO₂ Catalysts during Methane Oxidation. *Ind. Eng. Chem. Res.* **2019**, *58*, 12561–12570, doi:10.1021/acs.iecr.9b01267.

55. Ho, Y.-S.; Wang, C.-B.; Yeh, C.-T. Calorimetric study on interaction of dioxygen with alumina supported palladium. *J. Mol. Catal. A Chem.* **1996**, *112*, 287–294, doi:10.1016/1381-1169(96)00129-X.

56. Légaré, P.; Hilaire, L.; Maire, G.; Krill, G.; Amamou, A. Interaction of oxygen and hydrogen with palladium. *Surf. Sci.* **1981**, *107*, 533–546, doi:10.1016/0039-6028(81)90543-4.

57. Wrobel, R.J.; Becker, S.; Weiss, H. Influence of Subsurface Oxygen in the Catalytic CO Oxidation on Pd(111). *J. Phys. Chem. C* **2015**, *119*, 5386–5394, doi:10.1021/jp508952f.

58. Phan, D.Q.; Kureti, S. CO Oxidation on Pd/Al_2O_3 Catalysts under Stoichiometric Conditions. *Top. Catal.* **2017**, *60*, 260–265, doi:10.1007/s11244-016-0608-9.

59. Sheppard, T.L.; Price, S.W.T.; Benzi, F.; Baier, S.; Klumpp, M.; Dittmeyer, R.; Schwieger, W.; Grunwaldt, J.-D. In Situ Multimodal 3D Chemical Imaging of a Hierarchically Structured Core@Shell Catalyst. *J. Am. Chem. Soc.* **2017**, *139*, 7855–7863, doi:10.1021/jacs.7b02177.

60. Jones, J.; Xiong, H.; Delariva, A.T.; Peterson, E.J.; Pham, H.; Challa, S.R.; Qi, G.; Oh, S.; Wiebenga, M.H.; Pereira Hernández, X.I.; et al. Thermally stable single-atom platinum-on-ceria catalysts via atom trapping. *Science* **2016**, *353*, 150–154, doi:10.1126/science.aaf8800.

61. Trovarelli, A. Catalytic Properties of Ceria and CeO_2-Containing Materials. *Catal. Rev.* **1996**, *38*, 439–520, doi:10.1080/01614949608006464.

62. Suchorski, Y.; Wrobel, R.; Becker, S.; Weiss, H. CO Oxidation on a $CeO_x/Pt(111)$ Inverse Model Catalyst Surface: Catalytic Promotion and Tuning of Kinetic Phase Diagrams. *J. Phys. Chem. C* **2008**, *112*, 20012–20017, doi:10.1021/jp806033v.

63. Lott, P.; Eck, M.; Doronkin, D.E.; Popescu, R.; Casapu, M.; Grunwaldt, J.-D.; Deutschmann, O. Regeneration of Sulfur Poisoned $Pd–Pt/CeO_2–ZrO_2–Y_2O_3–La_2O_3$ and $Pd–Pt/Al_2O_3$ Methane Oxidation Catalysts. *Top. Catal.* **2019**, *62*, 164–171, doi:10.1007/s11244-018-1121-0.

64. Kim, J.; Kim, C.; Choung, S.-J. Comparison studies on sintering phenomenon of diesel oxidation catalyst depending upon aging conditions. *Catal. Today* **2012**, *185*, 296–301, doi:10.1016/j.cattod.2011.09.021.